END

FILMED

DTIC

		1.0		4.5	2.8	2.5
				5.0		
				5.6	3.2	2.2
				6.3	3.6	
		1.1		7.1	4.0	2.0
						1.8
		1.25			1.4	1.6

MICROCOPY RESOLUTION TEST CHART

NATIONAL BUREAU OF STANDARDS – 1963 – A

SECURITY CLASSIFICATION OF THIS PAGE *(When Data Entered)*

REPORT DOCUMENTATION PAGE		READ INSTRUCTIONS BEFORE COMPLETING FORM
1. REPORT NUMBER AFOSR-TR- 8 5 - 0 7 3 3	2. GOVT ACCESSION NO.	3. RECIPIENT'S CATALOG NUMBER
4. TITLE *(and Subtitle)* Improved Lifetime High Voltage Switch Electrodes		5. TYPE OF REPORT & PERIOD COVERED Final Technical 1 Sep 84 - 31 May 85
		6. PERFORMING ORG. REPORT NUMBER FR-60053
7. AUTHOR(s) Ward Halverson		8. CONTRACT OR GRANT NUMBER(s) F49620-84-C-0120
9. PERFORMING ORGANIZATION NAME AND ADDRESS SPIRE CORPORATION Patriots Park Bedford, MA. 01730		10. PROGRAM ELEMENT, PROJECT, TASK AREA & WORK UNIT NUMBERS 6110 2F 2301 /A7
11. CONTROLLING OFFICE NAME AND ADDRESS Air Force Office of Scientific Research Building 410 Bolling AFB, DC 20332		12. REPORT DATE 28 June 1985
		13. NUMBER OF PAGES
14. MONITORING AGENCY NAME & ADDRESS(if different from Controlling Office)		15. SECURITY CLASS. (of this report) Unclassified
		15a. DECLASSIFICATION DOWNGRADING SCHEDULE

16. DISTRIBUTION STATEMENT *(of this Report)*

Approved for public release; distribution unlimited.

17. DISTRIBUTION STATEMENT *(of the abstract entered in Block 20, if different from Report)*

18. SUPPLEMENTARY NOTES

19. KEY WORDS *(Continue on reverse side if necessary and identify by block number)*

Spark switches, electrodes, ion implantation.

20. ABSTRACT *(Continue on reverse side if necessary and identify by block number)*

In this Phase I Small Business Innovation Research (SBIR) program, preliminary tests of ion implantation to increase the lifetime of spark switch electrodes have indicated that a 185 keV carbon ion implant into a tungsten-copper composite has reduced electrode erosion by a factor of two to four. Apparently, the thin layer of tungsten carbide (WC) has better thermal properties than pure tungsten; the WC may have penetrated into the unimplanted body of the electrode by liquid and/or solid phase

DD FORM 1 JAN 73 1473 EDITION OF 1 NOV 65 IS OBSOLETE   Unclassified

AD-A158 961

DTIC FILE COPY

DTIC
SELECTED
SEP 1 1 1985
E

85 09 09 015

20. cont'd

diffusion during erosion testing. These encouraging results should
provide the basis for a Phase II SBIR program to investigate further
the physical and chemical effects of ion implantation on spark gap
electrodes and to optimize the technique for applications.

FINAL REPORT

SMALL BUSINESS INNOVATION RESEARCH PROGRAM

PHASE I

IMPROVED LIFETIME HIGH VOLTAGE SWITCH ELECTRODES

Contract No. F49620-84-C-0120

Submitted by:

SPIRE CORPORATION

Patriots Park

Bedford, MA. 01730

Ward Halverson, Principal Investigator

Submitted to:

Air Force Office of Scientific Research/XOT

Bolling AFB, DC 20332

In the Phase I program, we have investigated the technique of ion implantation to reduce the erosion of the electrodes in a high power spark gap. Energetic carbon and boron ions were implanted into the tunsten-copper electrodes of a spark switch and tested in a high-voltage discharge circuit. Tungsten carbide formed by ion implantation has considerably higher enthalpy to melt and higher thermal diffusivity than pure tungsten. Although these thermal properties are not available for tungsten borides, we believed that they were comparable to those of tungsten carbide. The electrode erosion tests showed mass removal rates of 30 to 44 micrograms per coulomb on the unimplanted and boron-implanted spark gap electrodes. The carbon-implanted electrodes, on the other hand, showed a factor of 2 to 4 less mass loss. Surface analysis indicated that melting and ejection of molten material were the major causes of the electrode erosion, the carbon-implanted electrodes had less melting of the tungsten component of the W-Cu matrix and less total loss of the electrode material than the other samples. These encouraging results should form the basis for a Phase II program in which ion implantation techniques for improving spark switch electrode lifetime are further investigated and optimized.

Potential applications of erosion resistant electrodes include spark switches in the power supplies of advanced pulsed laser and accelerator weapon systems, electromagnetic (rail gun) launchers, and in laser and accelerator systems for metalworking. Additionally, improved electrode materials could dramatically increase the lifetime of high current commutators, brushes and lightning arrestors.

TABLE OF CONTENTS

TABLE OF CONTENTS (concluded)

LIST OF ILLUSTRATIONS

LIST OF TABLES

SECTION 1
INTRODUCTION

High power spark switches represent a very important part of pulsed power technology because they have the capability of changing rapidly from the "open" state, holding off voltages up to many megavolts, to the "closed" state, in which hundreds to thousands of kiloamperes are conducted. Although there are some switching technologies which approach the voltage, current, or di/dt capabilities of spark switches (e.g., saturable magnetic reactors, ignitions, and high power vacuum tubes), none has the combined high voltage, high current, low inductance and low cost characteristics of spark gaps.

There are several advanced weapon system concepts which depend on high-performance switching or arc commutation for their operation. High-power pulsed lasers and electron accelerators require several spark switches in their Marx generators or pulse shaping circuits. Electromagnetic launchers (rail guns) may have spark switches in their power supplies and also may face severe erosion problems from arcing along the projectile's path. In the commercial area, pulsed laser machining and welding are beginning to be accepted for certain manufacturing operations. These lasers have pulsed power supplies which often rely on spark switching; the laser cavity is also strongly influenced by the interactions of energetic discharge plasmas with internal electrodes.

At present, electrode erosion is the major factor in determining the lifetime of a spark switch. Erosion changes the profile of the switch electrodes, thus changing the voltage holdoff, triggering characteristics, and series impedance of the switch. Additionally, the eroded material may be deposited on internal insulators, thereby inducing pretriggering and erratic voltage holdoff. High performance spark switches are normally rated by the number of coulombs which can be transferred before switch degradation. This rating usually translates into the range of 10^6 to 10^7 pulses for typical applications in lasers or electron accelerators. At 10^3 Hertz, 10^7 pulses are generated in only 2.8 hours. At the end of its lifetime, a switch must be completely or partially replaced, which is often a long, difficult task when the switch is located inside of a large, oil filled pulse generator.

A lifetime increase by a factor of 10 or more, to bring spark switches to the 10^8 to 10^9 pulse regime, would mean that a system pulsing at a repetition rate of 10^3 Hertz could operate for tens to hundreds of hours without maintenance.

The Phase I program reported here has addressed the spark switch erosion problem by investigating a technique which could greatly reduce the erosion of spark switch electrodes. Ion implantation to introduce a beneficial element or compound into the surface of a host material has been shown to reduce wear, corrosion and erosion in mechanical systems. The technique has been applied to the surface of spark gap electrodes. Although initially a surface modification, influencing only a few hundred nanometers of depth, the implanted material can migrate into the bulk of the substrate by solid and liquid phase diffusion. Thus, the beneficial effects of the ion implantation can be expected to continue well after the surface layer of the spark switch electrode has been removed.

Results of the Phase I program indicate that the tungsten carbide formed by the implantation of energetic carbon ions into tungsten spark gap electrodes has improved the erosion resistance by a factor of two to four. It should be possible, by optimization in a Phase II program, to increase the spark switch electrode lifetime by an even greater amount.

SECTION 2

BACKGROUND

2.1 SPARK GAP ELECTRODE EROSION

A considerable amount of study has been devoted to the erosion of spark gap electrodes, principally in the United States and the Soviet Union. This work is reported in a number of publications and unpublished reports.[1-6] The most comprehensive review of the theoretical and experimental research on high power switches, including spark gap erosion, was undertaken by Burkes et al.[1] in 1978. This information is presently being updated by Burkes and will appear as a report in 1985 or 1986. A review specifically of electrode erosion, by A.L. Donaldson, will be available as a doctoral thesis which is presently under preparation at Texas Tech University.[7]

In spite of the extensive study of spark gap electrode erosion, there is little quantitative agreement on erosion rates and their dependences on the many parameters involved. The fact that so many parameters can be varied (e.g., current, voltage, pulse duration and shape, electrode material, electrode dimensions and shape, gas type, flow rate and pressure, etc.) makes the experimental and theoretical study of erosion phenomena very difficult.

For metal electrodes it is generally agreed that surface melting and ejection of the molten material is the primary erosion mechanism. (Carbon electrodes sublime or are lost by the removal of macroscopic particles.) The amount of material lost generally appears to scale as the total number of coulombs transferred by the gap and is inversely proportional to the specific heat and melting temperature of the electrode material.[1] To first approximation, the temperature of a rapidly heated electrode, which determines the volume of melted material, varies inversely as the thermal diffusivity, $K/c_p \, \rho$, where K is the thermal conductivity, ρ is the density, and c_p is the specific heat of the material.

From the above discussion, an ideal electrode material should have high specific heat, melting temperature, thermal conductivity and diffusivity, heat of fusion, and electrical conductivity. Table 2-1 compares the physical properties of tungsten and the two of its refractory compounds studied in this program.[8,9] It can be seen that tungsten

-3-

TABLE 2-1.   PROPERTIES OF TUNGSTEN AND REFRACTORY TUNGSTEN
             COMPOUNDS

Tungsten:

Density	19.3 g/cm^3
Melt Temperature	3377°C
Heat of Fusion	43.5 cal/g
Heat Capacity at 25°C	.032 cal/g°c
Thermal Conductivity at 25°C	.43 cal/sec cm°C
Enthalpy for Melt from 25°C	184 cal/g
Thermal Diffusivity at 3377°C	0.021 cm^2/g
Resistivity at 20°C	5.5 micro-ohm-cm

Tungsten Carbide:

Density	15.7 g/cm^2
Melt Temperature	2777°C
Heat of Fusion	74.6 cal/g
Heat Capacity at 25°C	.051 cal/g°C
Thermal Conductivity at 25°C	.069 cal/sec cm°C
Enthalpy for Melt from 25°C	271 cal/g
Thermal Diffusivity at 2777°C	0.123 cm^2/g
Resistivity at 20°C	50-80 micro-ohm-cm

Tungsten Boride:

Density	10.77 g/cm^3
Melt Temperature	2820°C
Resistivity	21 micro-ohm-cm
Other data not available	

carbide has a significantly greater enthalpy required to melt (heating to melting point plus heat of fusion) and higher thermal diffusivity than pure tungsten. The thermal conductivity of WC, however, is considerably lower than for pure W, but it is not known whether this parameter is as important as the others. These parameters are not available for tungsten borides, although by analogy with WC, we believe that the enthalpy to melt and thermal diffusivity are larger and the thermal conductivity less than for pure W.

2.2   ION IMPLANTATION TO FORM TUNGSTEN CARBIDES AND BORIDES

Tungsten carbides and borides are among the hardest materials and would be very difficult to form into spark gap electrodes. Instead, we have used implantation by a beam of carbon or boron ions to form a thin layer of tungsten carbide or tungsten boride on electrodes which consist primarily of pure tungsten. (In the actual experiments, we used sintered W-Cu materials for reasons explained in Section 4.1.)

The principles of ion implantation are illustrated in Figure 2-1. An ion accelerator operating with a carbon or boron compound forms a beam of ions which is accelerated and mass analyzed to remove all but C^+ or B^+ ions, and this beam falls on the surface of the substrate. Depending on the energy, the beam particle, and the substrate material, the ions bury themselves in the substrate and form chemical compounds with the host material. If we assume that the ions are uniformly distributed throughout a layer of this thickness, then the ratio of the implanted particle density to the host particle density is given approximately by:

$$f \; = \; \frac{JM}{RA} \tag{1}$$

In Equation 1, J is the total fluence of implanted ions (cm^{-2}), R is the range of the ions, projected on a normal to the surface ($g \; cm^{-2}$), M is the molecular weight of the host material (g), and A is Avagadro's number (6.02×10^{23} per g mole).

For 200 keV carbon or boron ions incident on tungsten, the projected range is about $3.8 \times 10^{-4} \; g \; cm^{-2}$ (0.2 μm). An ion implant of $10^{18} \; cm^{-2}$ should then produce an implant/tungsten ratio of about 0.8, high enough to produce significant quantities of all types of tungsten carbide or tungsten boride. Even higher concentrations can be formed

with carbon or boron. The B-implanted Type 10W30 anode, which has a slightly higher tungsten concentration than 10W3, has about a factor of five lower weight loss rate, even though the weight change of the cathode (unimplanted Type 10W3) is about the same as for the control.

TABLE 5-1.   WEIGHT CHANGE OF SPARK GAP ELECTRODES

Electrode Type	Implant	Number of Pulses	Weight Change (mg)	Change per Coulomb (μg/Cb)
10W3 Anode	None	1.0×10^5	-2.2	-30.0
10W3 Cathode	None	1.0×10^5	-0.7	-9.6
10W3 Anode	C	1.02×10^5	-1.5	-16.3
10W3 Cathode	C	1.02×10^5	-0.8	-8.7
10W3 Anode	B	5×10^4	-0.6	-15.6
10W3 Cathode	B	5×10^4	+0.4	+10.4
30W3 Anode	B	1.00×10^5	-0.5	-5.6
10W3 Cathode	None	1.00×10^5	-0.8	-8.9

The only anomalous result is the apparent _increase_ of the mass of the B-implanted cathode exposed to 5×10^4 shots. This may represent an error in recording the weight of the electrode before testing.

The observed mass losses per coulomb are in the same range as those reported by J. J. Moriarty et al.[12] for erosion tests of Type 10W3 Elkonite.

5.3   SURFACE PROFILOMETRY

5.3.1   Anode Crater Volumes

The craters of the anode electrodes were examined by a Sloan Dektak I in an attempt to correlate the weight loss of the electrodes to visible surface damage. The profiles of the unimplanted anode and the carbon-implanted anode craters are compared in Figure 5-1. The descending trend of the reference line outside the crater is caused by a gentle rounding of the anode itself, away from the center of the electrode.

-19-

SECTION 5
RESULTS

5.1   VISUAL INSPECTION

5.1.1   Cathode Electrodes

None of the cathodes show visible signs of erosion after testing. However, a blackened area has appeared around the triggering hole (Figure 4-2) on all the tests, along with some discoloration of the original polished metallic surface.

The carbon-implanted cathode has considerably more discoloration than the others and bright, copper-colored spots about 1 mm in diameter are on the flat end and rounded shoulders of the electrode. No pitting, however, is visible on the surface. It appears that the spots represent copper transported from the anode electrode.

5.1.2   Anode Electrodes

All of the anodes have a single central crater with a width as large as 2 mm. Around the crater there is a ring of apparently ejected material with a width of 2 to 3 mm, depending on the sample. The rest of the surface of the anode is somewhat darkened but has no visible evidence of pitting.

The carbon-implanted anode appears rather different from the other electrodes. The central pit is smaller in diameter and depth than the others (see Section 5.3), and there is considerable evidence that the copper matrix of the Elkonite has been selectively ejected from the crater. Copper-colored spots with diameters of about 1 mm, similar to those on the cathode, were found on the flat surface and shoulders of the anode.

5.2   WEIGHT LOSS

The weight loss of the spark gap electrodes subjected to erosion testing showed a significant difference between implanted and unimplanted material. Table 5-1 gives the results of the weight loss measurements. There appears to be approximately a factor of two less weight loss per coulomb for the Type 10W3 Elkonite anodes which were implanted

4.3   TASK 3: ANALYSIS OF ELECTRODE EROSION

4.3.1 Weight Loss

The weight of each electrode and its mounting plate, as shown in Figure 4-2, was measured before and after the erosion tests by a Cenco laboratory balance with a reading accuracy of 0.1 mg. Handling and the process of mounting and demounting the electrode assemblies on the body of spark gap switch showed no effect on the measured weight.

4.3.2 Surface Profilometry

A Sloan Dektak I$^{(R)}$ was used to measure the dimensions of the visible crater found on the surface of the anode electrode after erosion testing. The volume of the crater was then compared to the weight change of the electrode.

4.3.3 SEM, EDS, and AES

Scanning electron micrography (SEM), energy dispersive spectroscopy (EDS), and Auger electron spectroscopy (AES) on the electrodes and samples, both before and after erosion testing, were performed at PhotoMetrics, Inc., of Woburn, Massachusetts.

Before testing, the polished surfaces of an unimplanted anode and a carbon-implanted anode were examined by SEM and EDS. Pre-test boron-implanted electrodes were not yet available for this analysis. After completion of the erosion testing, all samples were studied by SEM, EDS, and AES, including B-implanted coupons of 30W3 Elkonite. The results of these analyses are given in Section 5.4.

TABLE 4-4.   TEST CONDITIONS: C-IMPLANTED 10W3 ELECTRODES

Charging voltage: 27kV

Charge transfer per pulse: 9.0×10^{-4}Cb

Maximum current: 2.0 kA

Time to I_{max}: 260 ns

Pulse repetition rate: 5 s^{-1}

Spark gap pressure: 0.14 MPa (19.7 psi) dry air

Gas flow rate: 39 sccm

Total number of pulses: $1.02 \times 10^5 \pm 2.1 \times 10^3$

Total charge transfer: 91.8 ± 1.9 Cb

TABLE 4-5.   TEST CONDITIONS: B-IMPLANTED 30W3 ELECTRODE

Charging voltage: 27 kV

Charge transfer per pulse: 9.0×10^{-4} Cb

Maximum current: 2.0 kA

Time to I_{max}: 260 ns

Pulse repetition rate: 5 s^{-1}

Spark gap pressure: 0.14 MPa (22.7 psi) dry air

Gas flow rate: 39 sccm

Total number of pulses: $1.00 \times 10^5 \pm 1 \times 10^3$

Total charge transfer: 90.0 ± 0.9 Cb

TABLE 4-2.   TEST CONDITIONS: UNIMPLANTED 10W3 ELECTRODES

Charging voltage: 22 kV

Charge transfer per pulse: 7.3×10^{-4} Cb

Maximum current: 1.70 kA

Time to I_{max}: 260 ns

Pulse repetition rate: 18 s^{-1}

Spark gap pressure: 0.16 MPa (22.7 psi) dry air

Gas flow rate: 32 sccm

Total number of pulses: $1 \times 10^{5} \pm 2 \times 10^{3}$

Total charge transfer: 73.3 $\pm$ 1.5 Cb

TABLE 4-3.   TEST CONDITIONS: B-IMPLANTED 10W3 ELECTRODES

Charging voltage: 23 kV

Charge transfer per pulse: 7.7×10^{-4} Cb

Maximum current: 1.75 kA

Time to I_{max}: 260 ns

Pulse repetition rate: 18 s^{-1}

Spark gap pressure: 0.16 MPa (22.7 psi) dry air

Gas flow rate: 32 sccm

Total number of pulses: $5 \times 10^{4} \pm 8 \times 10^{3}$
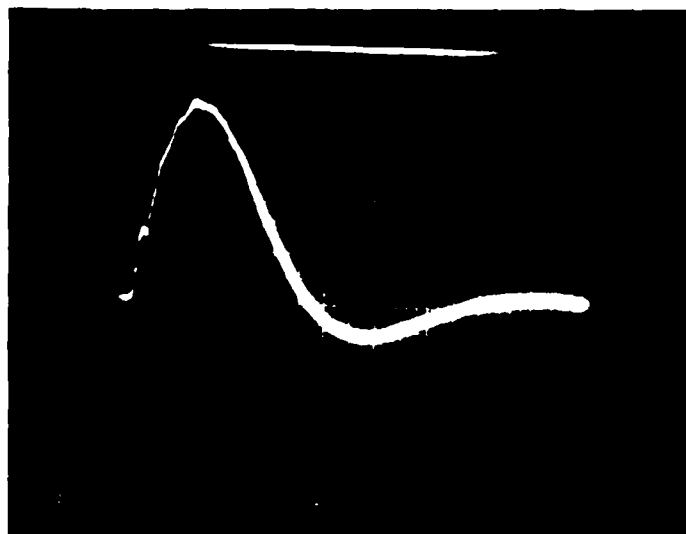
Total charge transfer: 38.5 $\pm$ 6.2 Cb

FIGURE 4-4. CURRENT WAVEFORM OF TESTING CIRCUIT
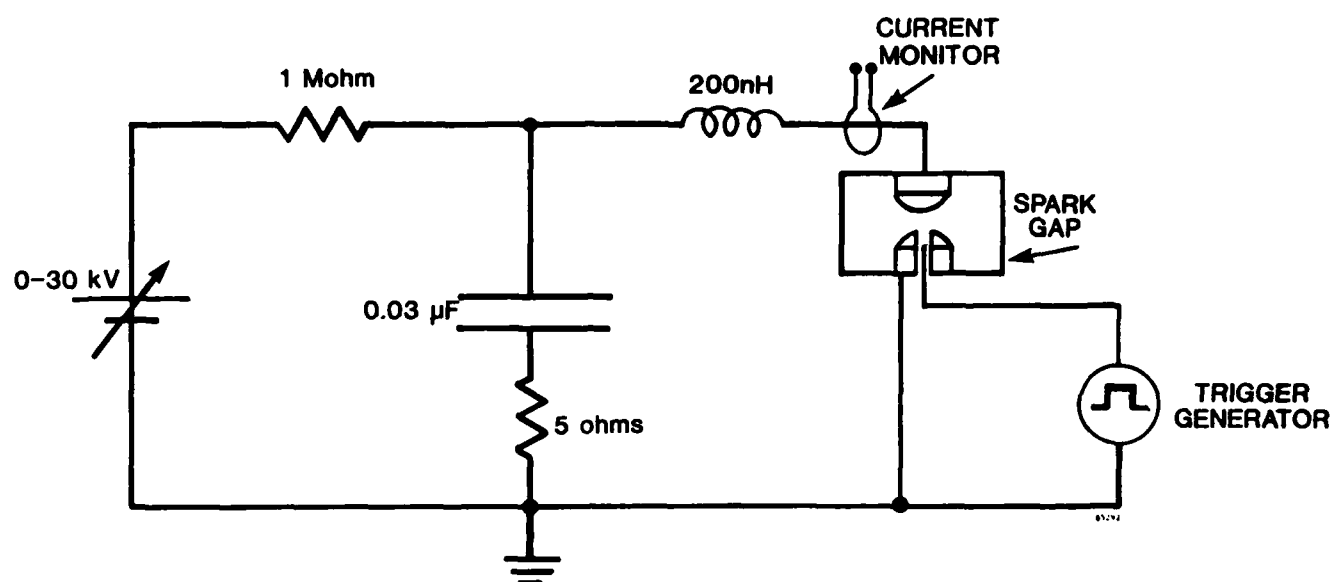(Horizontal: 200 ns/div. Vertical: 0.5 kA/div.)

FIGURE 4-3. SIMPLIFIED SCHEMATIC OF SPARK GAP TESTING CIRCUIT.

4.2.2 Erosion Test of Unimplanted Electrodes

The first test was performed on the unimplanted control electrodes for comparison with the implanted samples. The electrodes were weighed on a laboratory balance which can be read to an accuracy of 0.1 mg. The day-to-day repeatability of the balance is approximately $\pm$ 0.2 mg.

The conditions of the erosion test on the unimplanted electrodes are shown in Table 4-2.

4.2.3 Erosion Test of Boron-Implanted 10W3 Electrodes

The 10W3 Elkonite electrodes implanted with 1×10^{18} cm^{-2} of boron were tested next. The conditions of the test are shown in Table 4-3. The test was originally scheduled for 10^5 pulses for comparison with the results on the unimplanted electrodes, but the power supply of the testing circuit failed after $5 \times 10^4 \pm 8 \times 10^3$ shots. The uncertainty on the actual number of pulses is based on an approximately 15 minute uncertainty of the testing time. The B-implanted electrodes were removed from the spark switch after 5×10^4 pulses; the test was not continued because of the time constraints of the program.

4.2.4 Erosion Test of Carbon-Implanted 10W3 Electrodes

The 10W3 Elkonite electrodes implanted with 10^{18} cm^{-2} of carbon were subjected to a 10^5 shot erosion test after the power supply of the pulser was repaired. Table 4-4 summarizes the conditions of this test; the pulse repetition rate was set at 5 s^{-1} to reduce the heating of the high-voltage power supply. The higher accuracy quoted on the total charge transfer is also a result of the lower pulse repetition rate.

4.2.5 Erosion Test of Boron-Implanted 30W3 Electrode

As a result of the shortened test of the 10W3 electrodes (Section 4.2.3), it was decided to perform a second test of B-implanted material. The 30W3 electrode was used to provide a comparison with the somewhat less dense 10W3 Elkonite material (Table 4-1).

In this test, the B-implanted 30W3 anode was paired with an unimplanted cathode electrode, because it was observed in all previous testing (See Section 5.1 through 5.3) that little or no weight loss or visible damage occurred at the cathode. This test also produced essentially no erosion from the cathode. Table 4-5 summarizes the testing conditions.

-12-

TABLE 4-1.   PROPERTIES OF ELKONITE [R]

Type	Composition % by weight	atomic %	Density g cm^{-3}	Resistivity ohm cm	Thermal Conductivity W cm^{-1}°C^{-1}	Hardness Rockwell "B"
10W3	75 W; 25 Cu	51 W; 49 Cu	14.8	3.88×10^{-6}	2.6	98
30W3	80 W; 20 Cu	58 W; 42 Cu	15.6	4.21×10^{-6}	2.5	103

Source: CMW Incorporated, Indianapolis, Indiana

Identical 10^{18} cm^{-2} implants of B$^+$ were conducted on a second set of Tachisto 10W3 Elkonite spark gap electrodes and a Type 30W3 coupon following the apparently successful implant with carbon. A final B$^+$ implant of 10^{18} cm^{-2} was performed on a anode electrode machined from Type 30W3 Elkonite in Spire's shop. All of these implants resulted in visibly unchanged surfaces of the electrode material.

4.2   TASK 2: ELECTRODE TESTING

4.2.1   Test Circuit

The electrode erosion tests were all conducted on high-voltage pulser at Tachisto, Inc., which is used for "breaking in" new spark gap switches before shipment. The circuit diagram is shown in Figure 4-3. The inductance of the circuit, combined with the series resistance, produces a slightly underdamped waveform with a 0.26 microsecond risetime to peak current.

During electrode erosion tests, the capacitor bank was charged to a fixed voltage, in the range of 20 to 25 kV, and repetitively triggered at a preset rate of 5 to 20 s^{-1}. The total number of shots on the switch was then the product of the repetition rate and the test duration. Voltage, current, and repetition rate measurements were made periodically during the testing period. Figure 4-4 shows a typical current trace from the circuit taken during the testing of the spark gap electrodes.

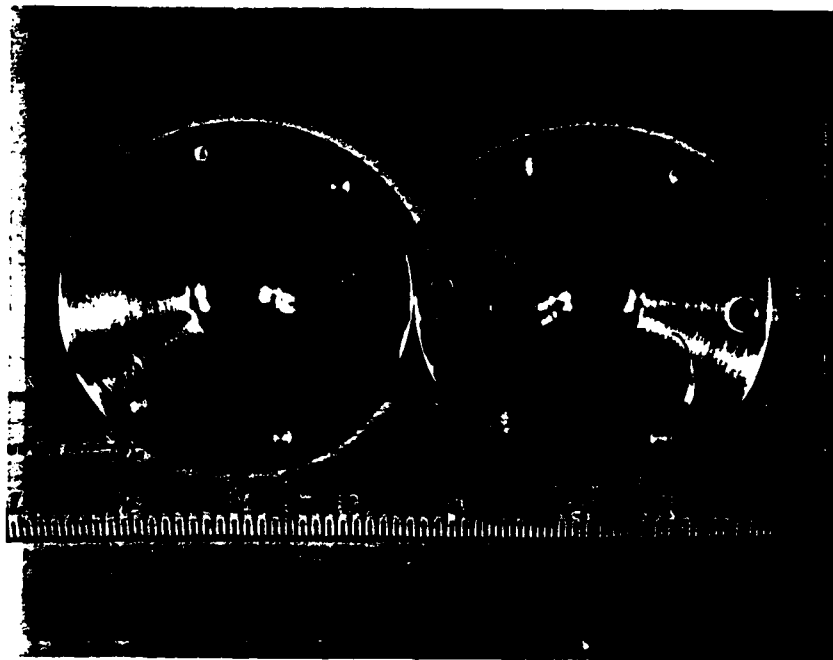FIGURE 4-1. TACHISTO SPARK GAP SWITCH.

FIGURE 4-2. SWITCH ELECTRODES.

SECTION 4
WORK PERFORMED

4.1   TASK 1: IMPLANTATION OF ELECTRODES

4.1.1   Electrodes and Spark Switch

The time constraints of the 6-month Phase I program forced a change of the electrode material to be tested. Machining of pure tungsten can only be performed in a few specifically equipped shops, and delivery schedules were unacceptably long for this program. It was decided to substitute sintered tungsten-copper for the pure tungsten and to use a commercially available design as the electrode configuration.

A spark gap switch with Elkonite[11] Type 10W3 electrodes was purchased from Tachisto, Inc., of Needham, MA, along with three extra sets of electrodes. The switch and electrodes are shown in Figures 4-1 and 4-2. The solid electrode is called the "anode" because it is usually on the positive side of a DC discharge circuit. The trigger electrode, called the "cathode," has a 4.8 mm diameter hole in the center which exposes the firing pin of an automobile spark plug. The discharge in the gap is initiated by a spark between the firing pin and the body of the electrode. The Elkonite electrodes are 22.2 mm diameter cylinders, with a 6.4 mm radius transition from the flat end to the cylindrical side. The minimum anode-cathode distance is fixed by the spark gap geometry at 10.2 mm.

In addition to the Type 10W3 Elkonite used by Tachisto, a 2.54 cm diameter bar of Type 30W3 was purchased for comparison. The composition of these materials is given in Table 4-1. There is very little difference between the two types.

4.1.2   Ion Implantation

A set of Tachisto spark gap electrodes and a 0.5 cm thick disk of Type 30W3 Elkonite were implanted with a total dose of 1×10^{18} cm^{-2} of carbon ions using Spire's equipment. Each sample was exposed to a 185 keV C$^+$ beam of 9.3×10^{-5} A/cm^2 for a period of 1700 s to produce this fluence. The power density at the surface of the samples was only 17 W/cm^2, and the electrodes could be kept close to room temperature during implantation by a substrate cooling system. There was no visible evidence of damage to the implanted surfaces by sputtering.

3.2.3 Task 3: Analysis of Electrode Erosion

The effect of ion implantation on the erosion of spark gap electrodes was to be determined in three ways. First, the weight loss of the implanted and control electrodes after a large number of discharge cycles was to be compared. Second, the surfaces of the electrodes were to be examined by scanning electron microscopy (SEM) and the nature of the damage and erosion determined. Finally, chemical analysis of the surface by Auger electron spectroscopy was to be performed to determine the carbon and boron concentration and depth profiles after pulsing.

SECTION 3
OBJECTIVES

3.1 OVERALL OBJECTIVE

The objective of the Phase I program was to demonstrate that ion implantation can reduce the rate of erosion of spark gap electrodes. To accomplish this objective, it is necessary to show two results. First, that there is a reduction of the eroded mass per coulomb of charge passing through a spark gap, and second, that the implanted material diffuses into the unimplanted substrate as part of the erosion process.

3.2 STATEMENT OF WORK

The objectives of the Phase I program were to be achieved by performing the following set of tasks:

3.2.1 Task 1: Implantation of Electrodes

Three sets of spark gap electrodes were to be fabricated from tungsten. One set was implanted th carbon, the second set implanted with boron, and the third left unimplanted as a control.

The depth profile of the implanted ions in the electrodes was to be determined by an analytical technique such as Auger electron spectroscopy of small coupons implanted along with the spark gap electrodes.

3.2.2 Task 2: Electrode Testing

A comparison of the performance of the carbon-implanted, boron-implanted and unimplanted tungsten electrodes was to be performed by using the electrodes in a spark gap switch. Each electrode pair was to be subjected to 10^5 discharges or more, at an electrical power level which can cause damage to tungsten switches.

The electrodes were to be operated at a pulse repetition rate of 10 Hz in an atmosphere of dry air, a typical spark switch insulating gas.

ENERGETIC IONS FROM
ION IMPLANTER

SUBSTRATE
SAMPLE

IMPLANTED IONS

TYPICAL ENERGY
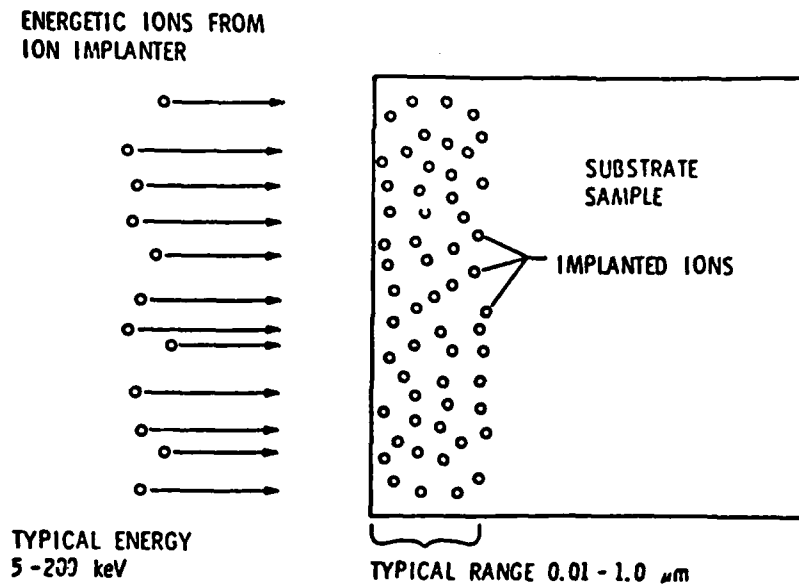5 -200 keV

TYPICAL RANGE 0.01 - 1.0 μm

FIGURE 2-1. ION IMPLANTATION. This process introduces isotopically pure
ions into the near surface region of materials. Alloys are formed
in the surface without altering the bulk properties.

by cascade implantation, in which a thin layer of pure boron or carbon is placed on the
surface of the substrate before implantation by the same material. The primary high
energy ions then "knock" some of the coating material into the substrate by recoil and add
to the total implanted dose. This technique is particularly useful when implanting into a
material which can be easily damaged by sputtering. For the case of tungsten substrates,
cascade implantation was not used because surface sputtering was not expected or
observed.

Because the implanted zone is very thin, typically less than 1 micrometer, it might
be assumed that the spark gap electrode would lose the benefits of the implantation as
soon as the surface layer has been eroded away. However, the erosion is a melting
process and the implanted material can mix with and diffuse into the unimplanted molten
tungsten. Part of this material is, of course, removed during each cycle, but a
considerable fraction of the original implant can migrate to deeper regions and preserve
the improved wear properties of the refractory tungsten carbide or tungsten boride
surface layer. This migration phenomenon has been observed in a number of experiments
on ion implanted steels.[10]

-6-
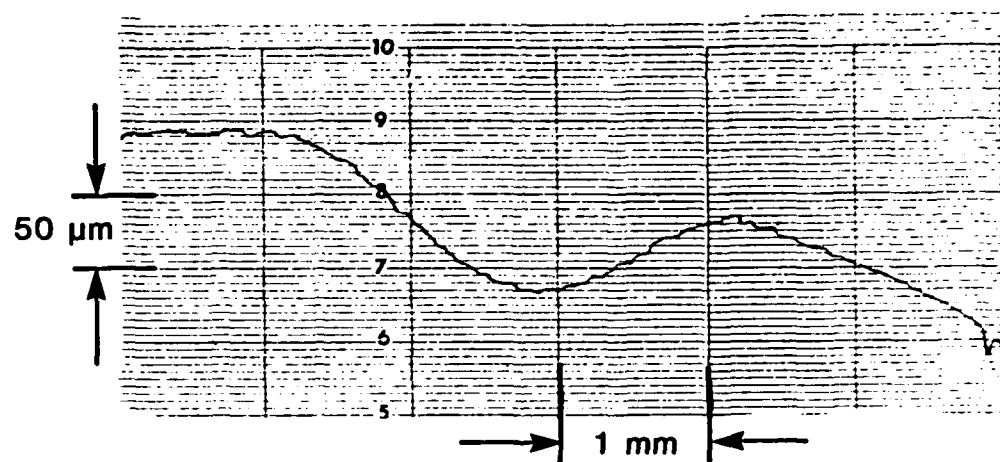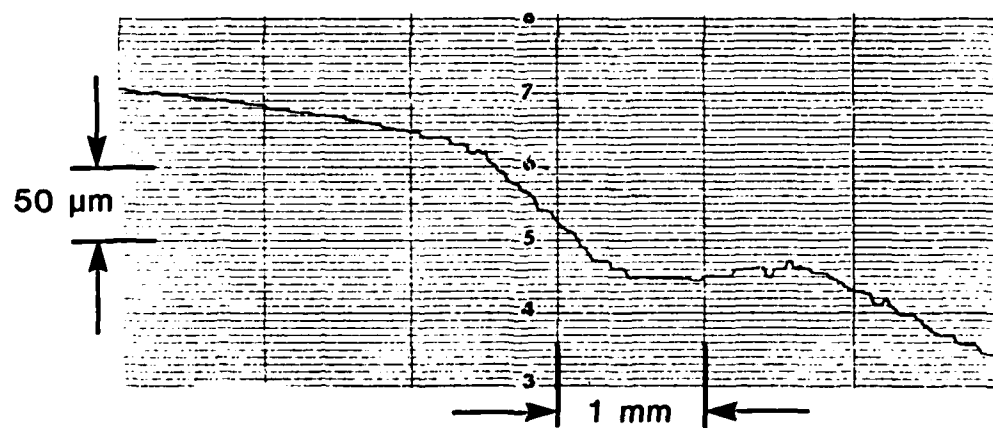
UNIMPLANTED ANODE

C-IMPLANTED ANODE

FIGURE 5-1. DEPTH PROFILES OF ANODE CRATERS.

The volumes of the craters were estimated by assuming that their shape is a paraboloid of revolution,

$$V = \frac{1}{2} \pi r^2 h$$

where h is the crater depth and r is its average radius. This formula is quite accurate for most shapes as long as $h^2 \ll r^2$. This is the case for all of the anode erosion craters.

The dimensions, estimated volumes and corresponding mass ejected from the central craters are shown in Table 5-2. The mass removed was calculated using a measured mass density of 12.6 g/cm^3 for 10W3 Elkonite and 13.2 g/cm^3 for 30W3 Elkonite. These values are somewhat less than the densities claimed by the manufacturer, shown in Table 4.1.

5.3.2 Comparison with Weight Losses

The estimated mass removed from the anode craters can be compared with the weight changes shown in Table 5-1. With the exception of the carbon-implant, the mass loss from the crater is considerably greater than the measured change of weight. We believe that this represents a redeposition of the ejected material on the surface of the electrode. Apparently the C-implanted electrode lost less electrode material from the central crater than the others, and it did not redeposit in as large quantities as the B-implanted or unimplanted material.

TABLE 5-2. ANODE CRATERS

Electrode Type	Crater Depth (cm)	Diameter (cm)	Estimated Volume (cm^3)	Est. Mass. Loss (mg)	Est. Loss/Coulomb (μg/Cb)
Unimplanted, 10^5 shots	8.5 x 10^{-3}	0.28	2.5 x 10^{-4}	3.2	44
C-Implant, 10^5 shots	5.0 x 10^{-3}	0.20	7.9 x 10^{-5}	1.0	11
B-Implant, 5 x 10^4 shots	7.0 x 10^{-3}	0.20	1.1 x 10^{-4}	1.4	36
B-Implant, 30W3, 10^5 shots	8.0 x 10^{-3}	0.28	2.4 x 10^{-4}	3.1	34

5.3.3 Crater Mass Loss Per Coulomb

As shown in Table 5-2, the estimated mass lost from the central crater per coulomb is lower by a factor of 4 in the C-implanted anode than from the unimplanted anode electrode. It is about a factor of 3 less than for the B-implants. This is a significant result of the experimental program.

5.4 SCANNING ELECTRON MICROSCOPY (SEM) AND ENERGY DISPERSIVE SPECTROSCOPY (EDS)

The spark gap anode electrodes were studied by SEM and EDS before and after the erosion testing. In the scanning electron microscopy, both secondary electron images (SEI) and Robinson backscatter electron images (RBEI) were made. The SEI micrographs are standard SEM showing principally the topography of the surface. RBEI micrographs are more sensitive to the composition of the material; brighter areas of the image usually correspond to concentrations of heavier elements, in this case, tungsten.

5.4.1 Before Erosion Testing

A new, unimplanted 10W3 Elkonite anode electrode was studied by SEM before testing. The surface of the electrode had been polished with a fine jeweler's rouge before this analysis. Figures 5-2 and 5-3 are SEI micrographs of the surface. Polishing scratches are quite evident, as are large inclusions of lower Z material, which is presumably copper.

An EDS analysis of the unimplanted electrode showed 53 at. % W and 47 at. % Cu (77% W; 23% Cu by Weight) which is close to the manufacturer's specifications (Table 4-1).

The 10W3 Elkonite anode implanted with 10^{18} cm^{-2} of carbon was also studied by SEM and EDS before erosion testing. Figure 5-4 is a SEI micrograph of its surface at a magnification comparable to that of Figure 5-2. It appears that the ion implantation process somewhat sputtered the electrode, "softening" the scratches and causing a general roughening of the surface. EDS of the surface showed 46 at % W and 54 at % Cu.
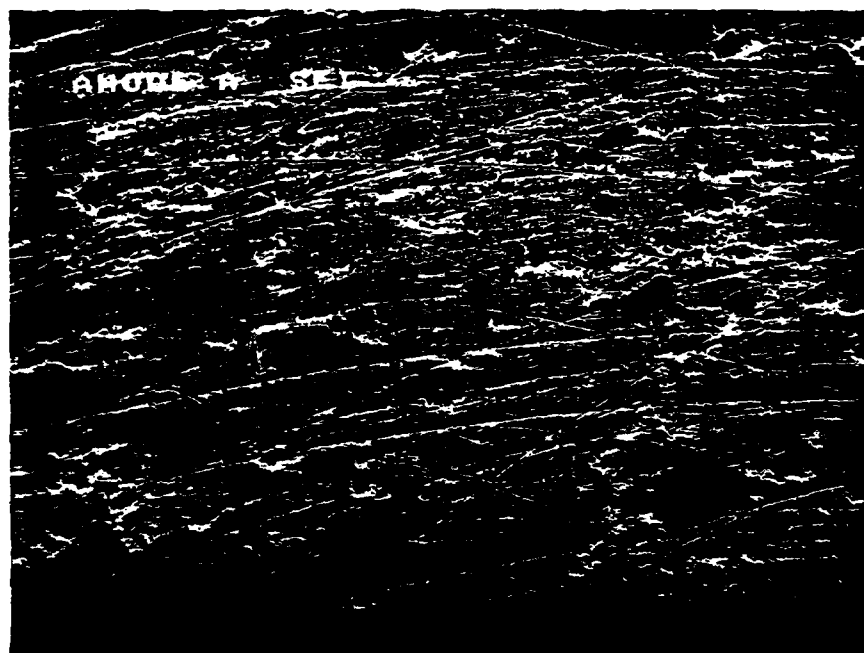
FIGURE 5-2. UNIMPLANTED 10W3 ANODE BEFORE EROSION TESTING
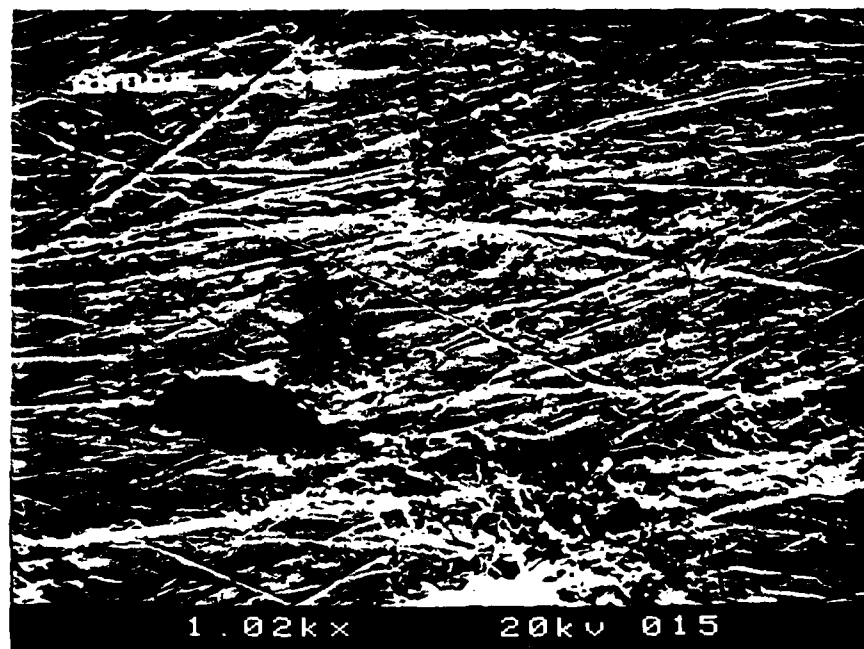(102X MAGNIFICATION).

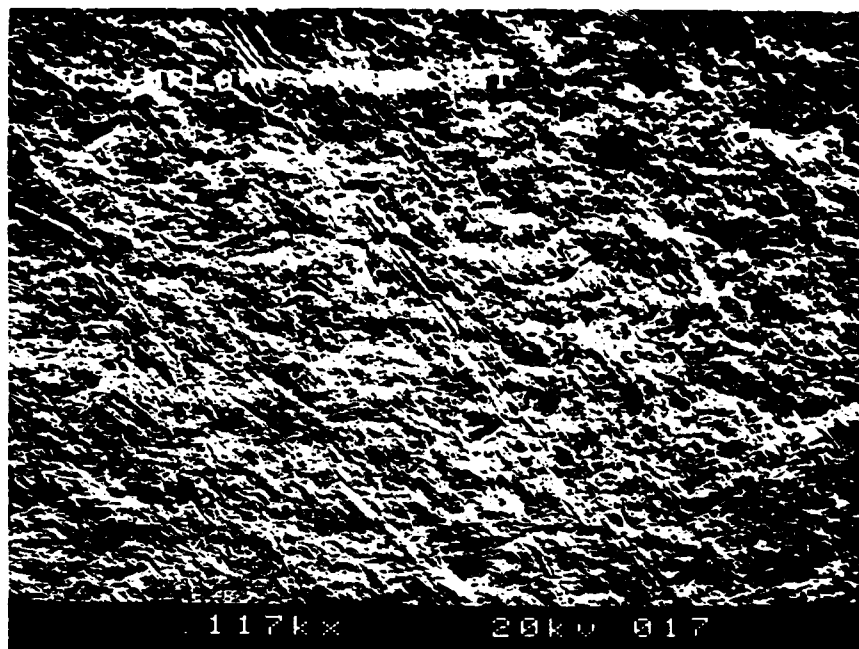FIGURE 5-3. MAGNIFICATION OF CENTER OF FIGURE 5-2 (1020X).

FIGURE 5-4. SEM OF CARBON-IMPLANTED 10W3 ANODE, BEFORE
EROSION TESTING (117X).

5.4.2 After Erosion Testing

Unimplanted Anode

SEM images of the unimplanted 10W3 Elkonite anode after 10^5 pulses are shown in Figures 5-5 through 5-7. The outside edges of the crater appear to have collected a considerable amount of ejected material. The RBEI micrograph of Figure 5-6 shows that a considerable amount of both high- and low-Z material was redeposited, almost completely covering the polishing scratches in the electrode.

In the center of the crater, Figures 5-7, there are clear indications of melting of both the tungsten and copper in the Elkonite matrix. This observation is confirmed by EDS analysis showing 69 at. % W; 31 at. % Cu in a "nodule" and 11 at. % W; 89 at. % Cu on a smooth, rounded surface of Figure 5-7.

C-Implanted Anode

The C-implanted anode, after 10^5 pulses, is shown in Figures 5-8 through 5-10. EDS analysis of the "splatter" outside the crater, Figure 5-9, shows a composition of 29 at. % W; 71 at. % Cu. The melted material inside the crater, Figure 5-10, has a composition of 89 at. % W; 11 at. % Cu.

-24-

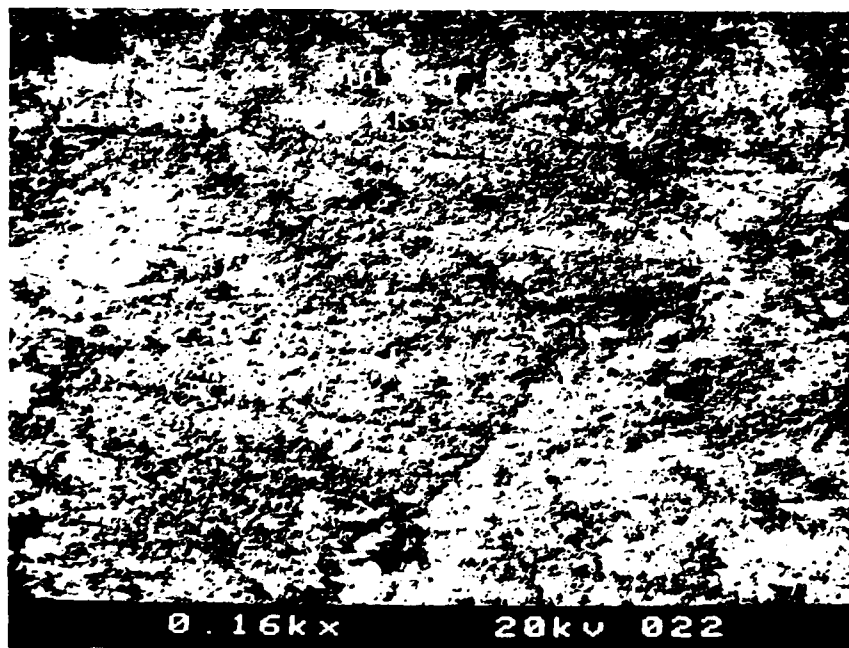FIGURE 5-5. CRATER IN UNIMPLANTED 10W3 ANODE AFTER 10^5 SHOTS (16X).

FIGURE 5-6. ROBINSON BACKSCATTER IMAGE (RBEI) OF UNIMPLANTED ANODE, OUTSIDE OF CRATER (160X).
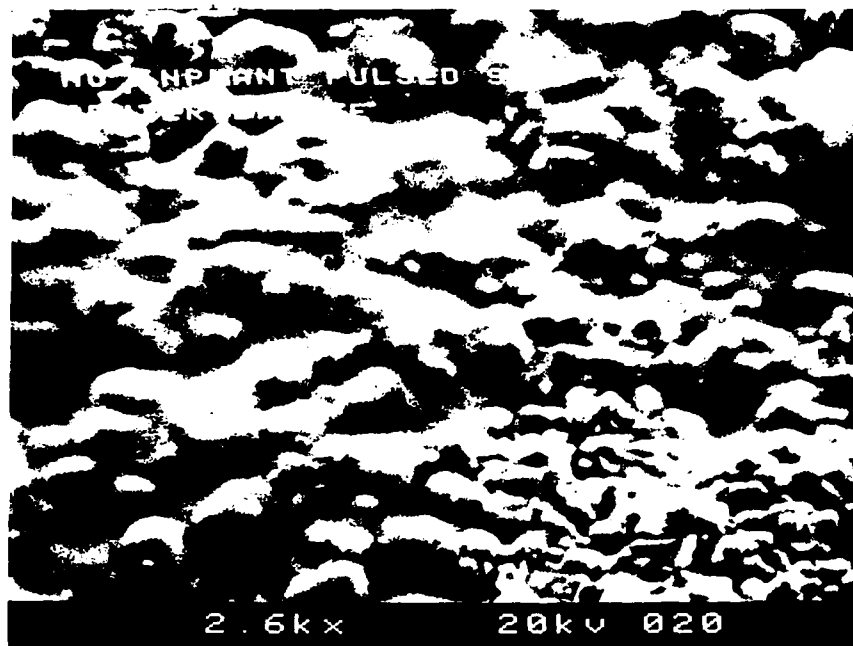
FIGURE 5-7. CENTER OF CRATER ON UNIMPLANTED ANODE (2600X).

FIGURE 5-8. RBEI OF C-IMPLANTED 10W3 ANODE AFTER 10^5 SHOTS (16X).

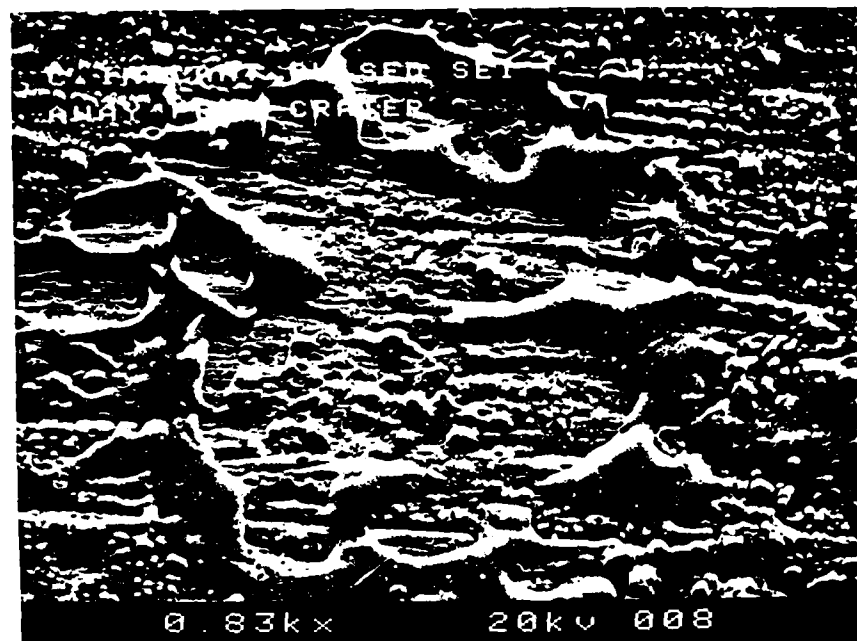FIGURE 5-9. SURFACE SPOT OUTSIDE OF CRATER IN C-IMPLANTED
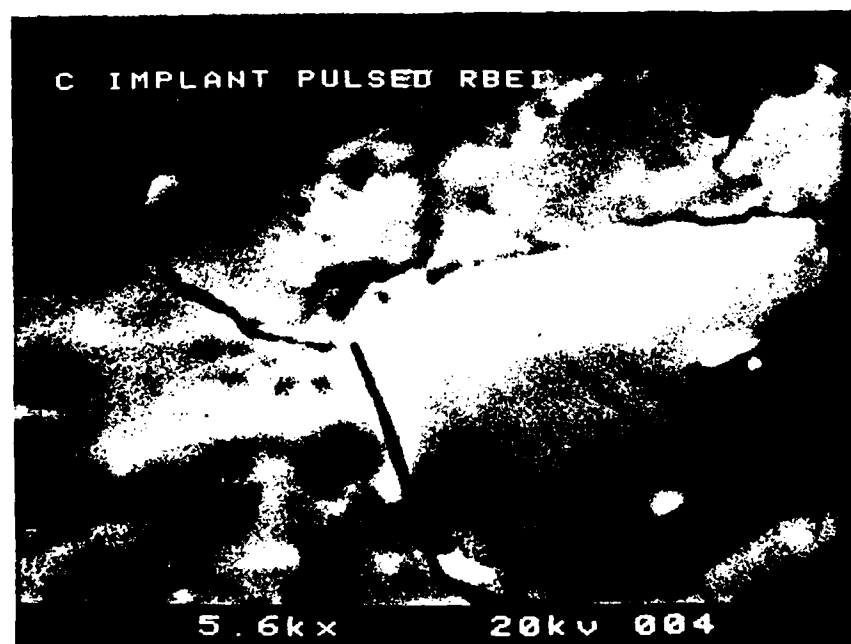ANODE (830X).

FIGURE 5-10. RBEI OF MELTED AREA INSIDE CRATER ON C-IMPLANTED
ANODE (5600X).

-27-

There is a qualitative difference between the erosion pattern on the C-implanted anode and on either the unimplanted anode or the B-implants, discussed below. In general, the C-implanted anode's central crater is smaller and the ejected material appears to have a higher concentration of copper than for the other electrodes. Additionally, EDS analysis of the material inside the crater shows a higher concentration of tungsten than for either the unimplanted or B-implanted cases.

B-Implanted Anodes

SEM photomicrographs of the 130W3 and 10W3 B-implanted anodes are shown in Figures 5-11 through 5-14. The 10W3 electrode was subjected to only 5×10^4 shots while the 30W3 anode was tested to the full 1×10^5 pulses.

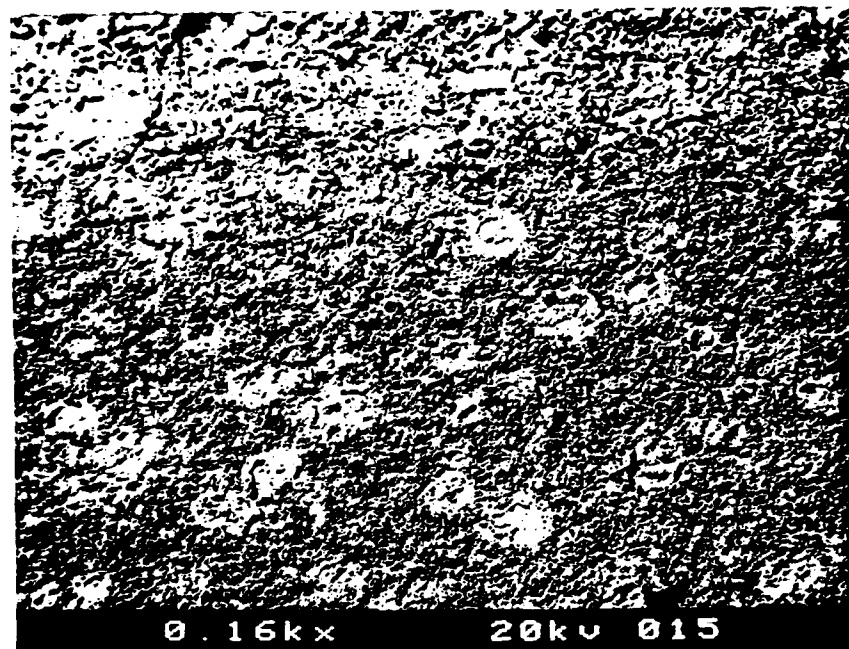FIGURE 5-11.   B-IMPLANTED 30W3 ELKONITE ANODE AFTER 10^5 SHOTS (16X).

-28-

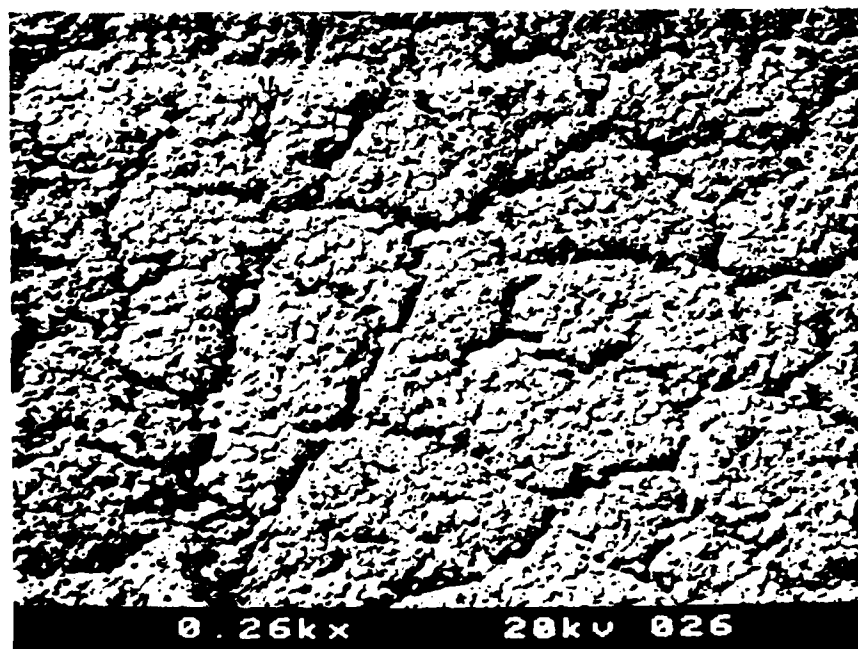FIGURE 5-12.   TUNGSTEN SURFACE SPLATTER AWAY FROM CRATER
SHOWN IN FIGURE 5-11 (160X).

FIGURE 5-13.   RBEI OF INNER EDGE OF 10W3 ANODE CRATER AFTER
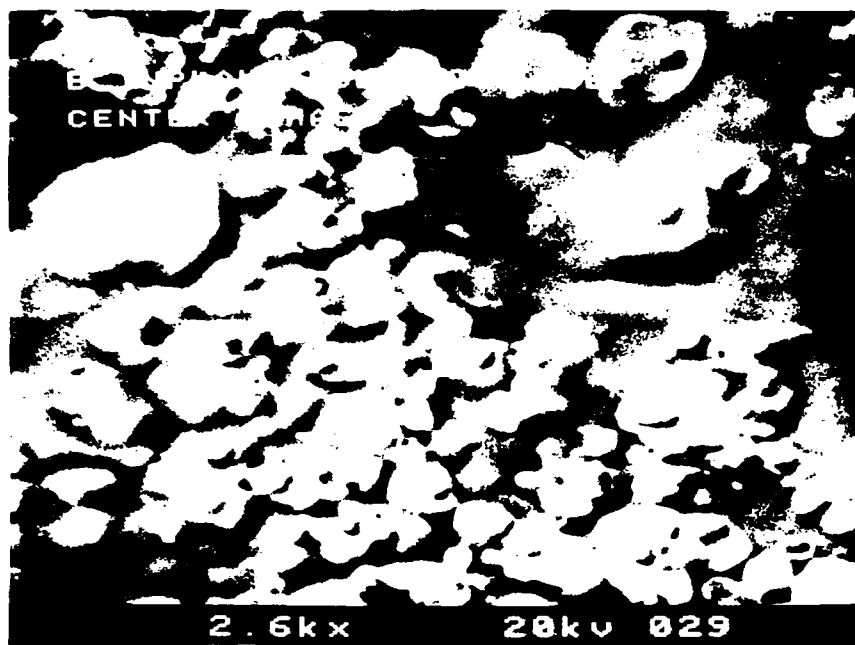5×10^4 SHOTS (260X).

FIGURE 5-14.   RBEI OF CRATER BOTTOM OF 10W3 ANODE (2600X).

The erosion of both electrodes was quite similar to that of the unimplanted anode, although the 10W3 anode which was pulsed only 5×10^4 times showed a pattern of cracking midway between the crater bottom and upper edge. EDS analysis of the ejected material outside the 10W3 crater showed a composition of 45 at. % W; 35 at. % Cu. A nodule on the inside of the crater had a composition of 73 at. % W; 27 at. % Cu. Very similar EDS results were obtained for the 30W3 anode. There appears to be very little qualitative or quantitative difference between the SEM or EDS results for the B-implanted and unimplanted anodes.

5.5   AUGER ELECTRON SPECTROSCOPY

AES was performed on four samples by PhotoMetrics, Inc., of Woburn, Massachusetts. The samples included the coupon of 30W3 Elkonite, analyzed on both the unimplanted and B-implanted faces, an unimplanted 10W3 anode after 10^5 shots and the C-implanted 10W3 anode after 10^5 shots.

The chemical composition of the samples was determined as a function of depth as the surface material of a small spot (less than 1 mm) diameter was sputter-etched by an argon ion beam. The etching rate on the W-Cu matrix is between 12.5 and 15 nm/min.[13].

-30-

Unimplanted Anode

Figure 5-15 shows the Auger electron spectrum for the unimplanted 10W3 anode at the center of the erosion crater. Figure 5-16 shows the profile of the identified elements as a function of depth in this location. There appears to be a peak in the copper concentration relative to tungsten which is centered about a depth of 100 nm.

C-Implanted Anode

Figure 5-17 gives the Auger spectrum from the center of the crater of the C-implanted 10W3 anode. There apparently is a higher concentration of carbon with respect to tungsten than for the unimplanted anode, although this could be only an effect of surface contamination. Figure 5-18 gives the depth profile of the identified elements in the C-implanted crater. It is clear that the tungsten concentration is considerably higher than in the virgin material. (See Table 4-4). In the 0 to 10 minute sputtering period (0-140 nm), the C-implanted anode also had a considerably higher concentration of W than in the implanted anode (Figure 5-16).

B-Implanted Control and Anode Electrodes

AES was performed on the 30W3 Elkonite control coupon implanted on one side with 185 keV boron ions to a dose of 10^{18} cm^{-2}. The Auger spectrum shown in Figure 5-19 is from the unimplanted side of the coupon. Carbon, nitrogen and oxygen represent surface contamination from handling, in spite of cleaning before the AES was performed. The B-implanted side was analyzed at depths up to about 125 nm, representing more than half the average range of 185 keV B$^+$ in W or Cu. Figure 5-20 is a high-resolution spectrum around the boron Auger line at 179 eV at a sputtering depth of about 70 nm. Unfortunately, the 179 eV W line lies on top of the B line and makes interpretation of the data quite difficult. However, the relative heights[14] of the peaks at 169 eV and 179 eV may indicate that some B is present in the matrix. However, the coincidence of the B and W identifying lines make quantitative AES analysis of the B profile in the eroded spark gap electrodes impractical, and further AES was discontinued for the B-implanted anodes.

FIGURE 5-15. AUGER ELECTRON SPECTRUM FROM CRATER OF UNIMPLANTED ANODE.
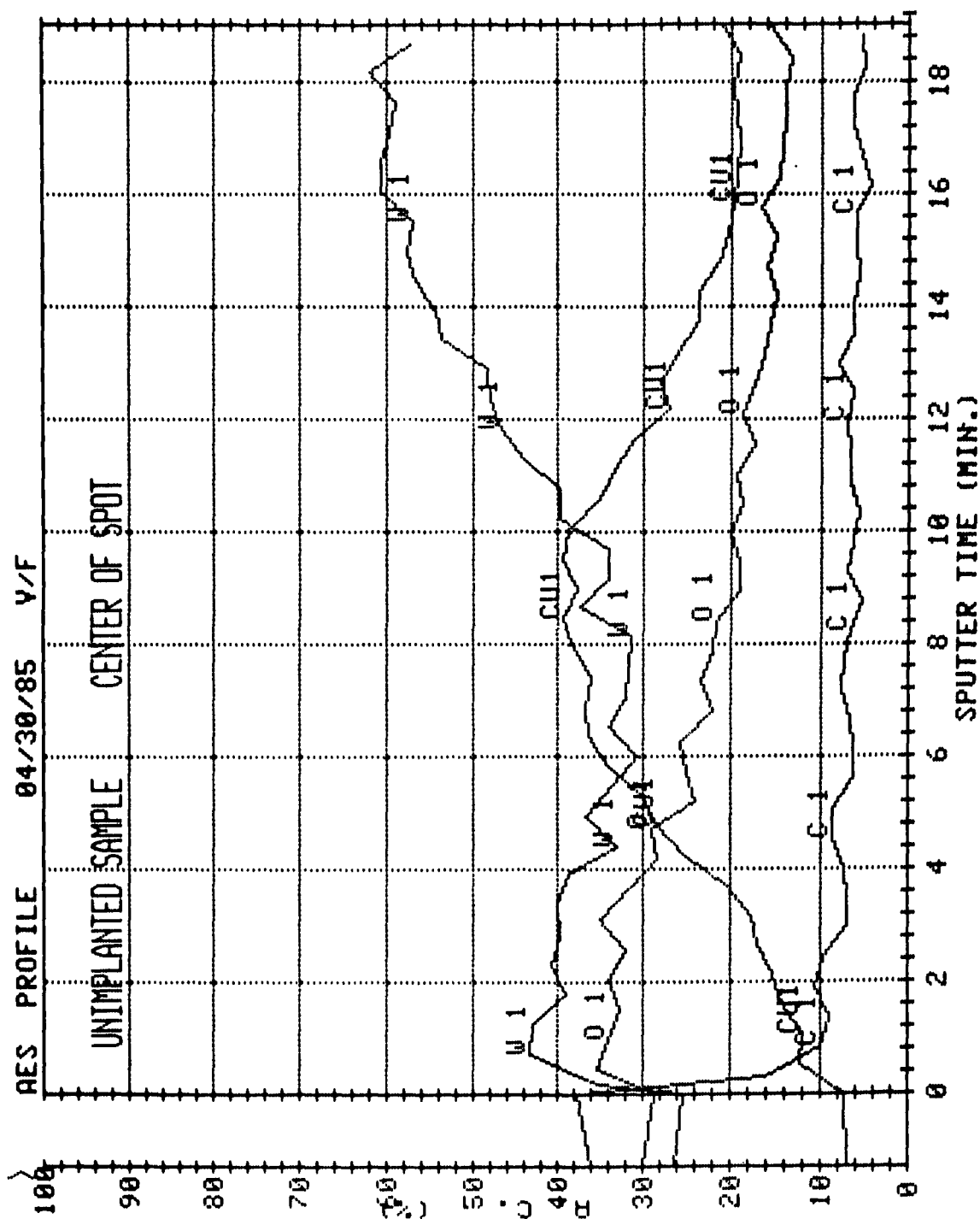
FIGURE 5-16. AES DEPTH PROFILE IN CRATER OF UNIMPLANTED ANODE. (Sputtering Rate: 12.5-15 nm/min.)

-33-

EXPANSION FACTOR=1.59   CARBON IMPLANT SAMPLE AS RECEIVED SURFACE

AES   SURVEY   SF=6.117, .000 DAT=2.00   04/30/85   V/F
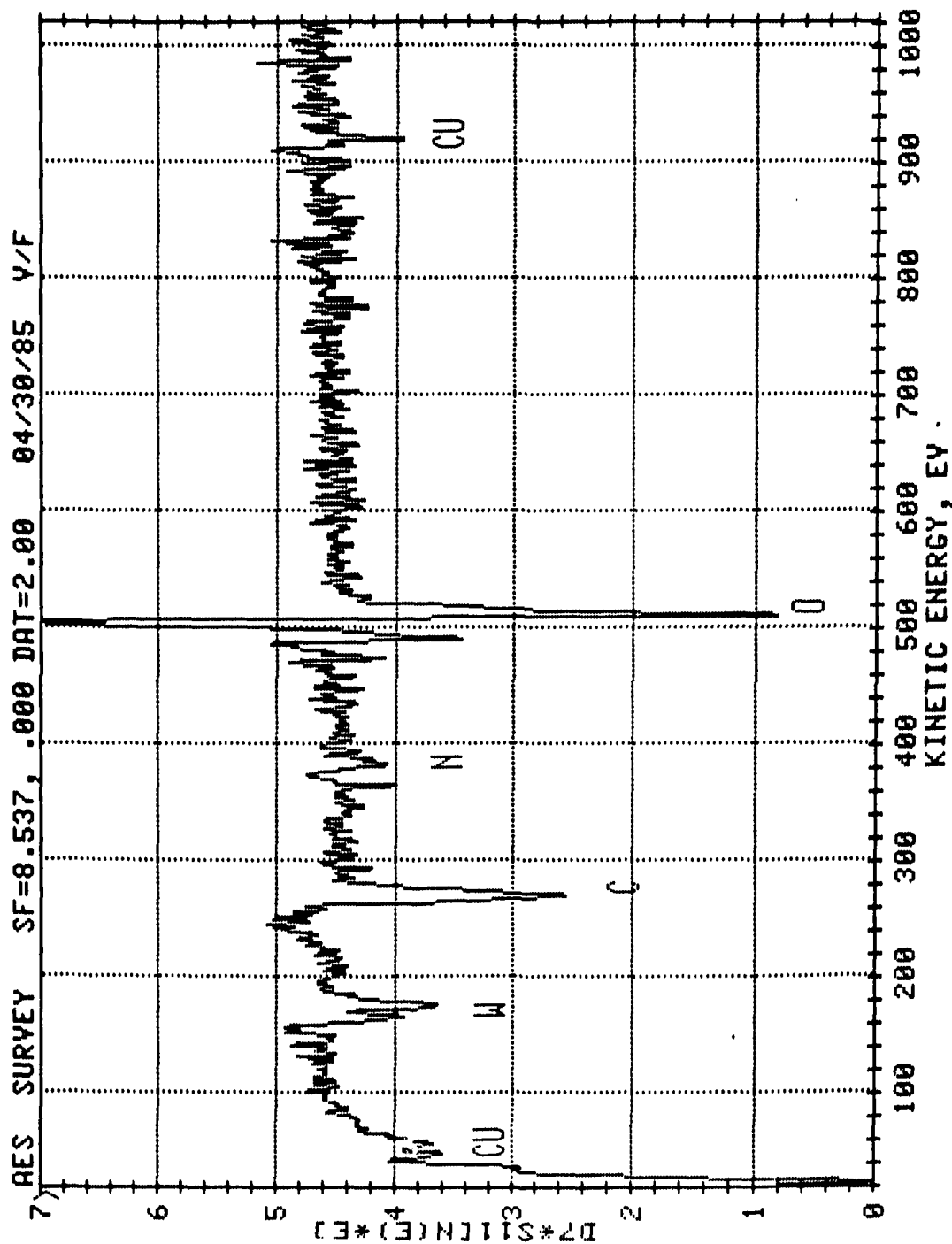

KINETIC ENERGY, EV

FIGURE 5-17.   AUGER ELECTRON SPECTRUM FROM CRATER OF
C-IMPLANTED ANODE.
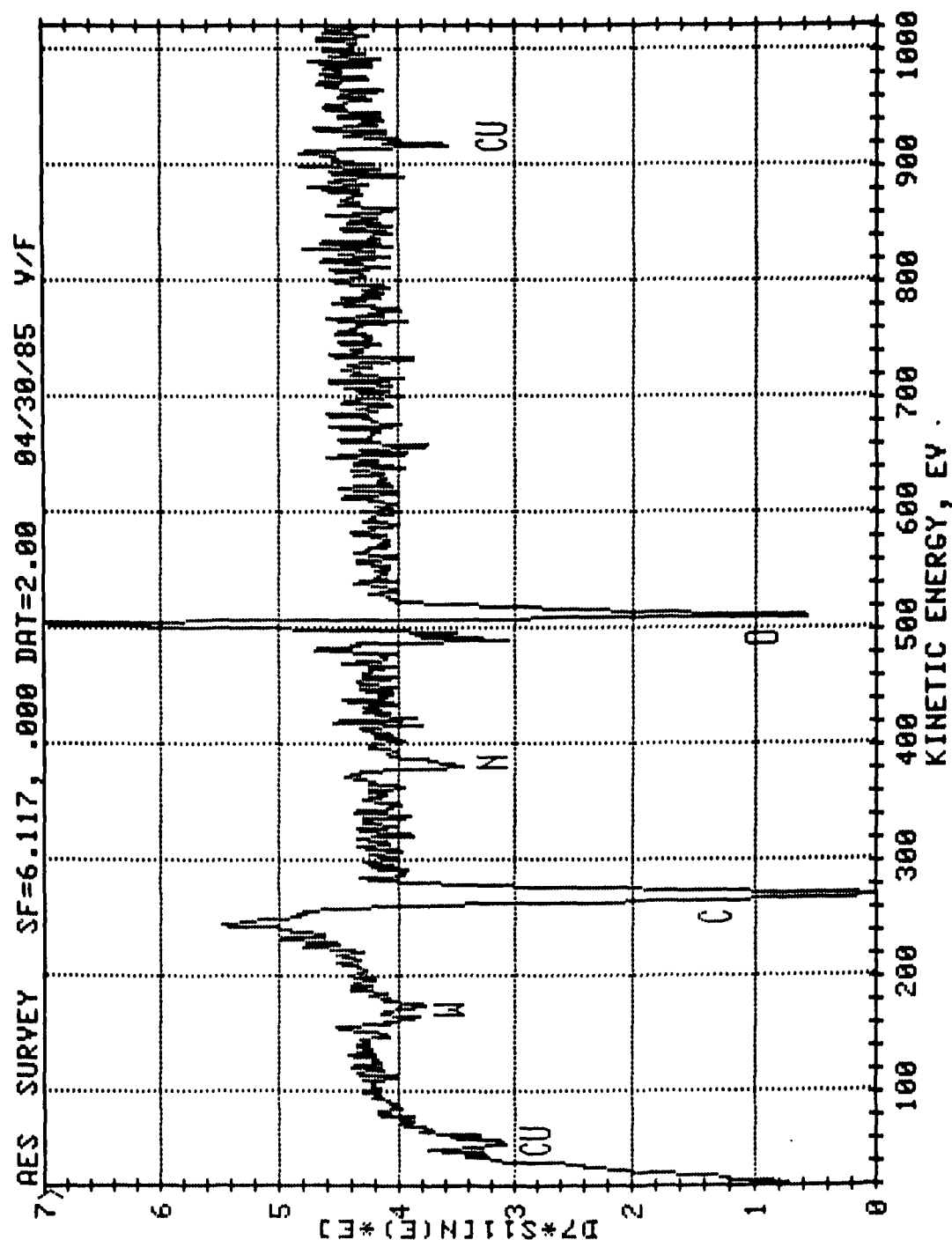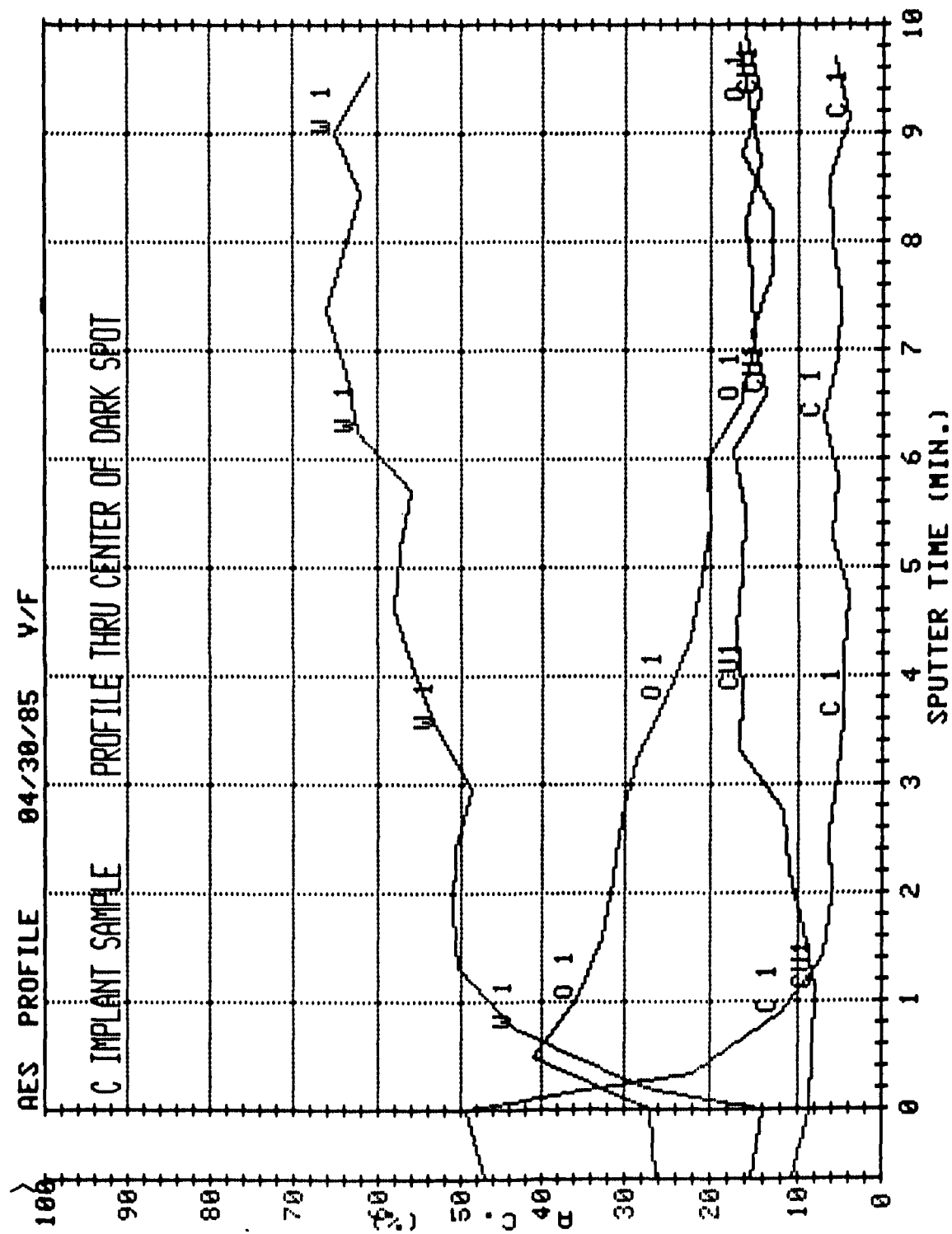
FIGURE 5-18. AES DEPTH PROFILE IN CRATER OF C-IMPLANTED ANODE. (Sputtering rate: 12.5–15 nm/min.)

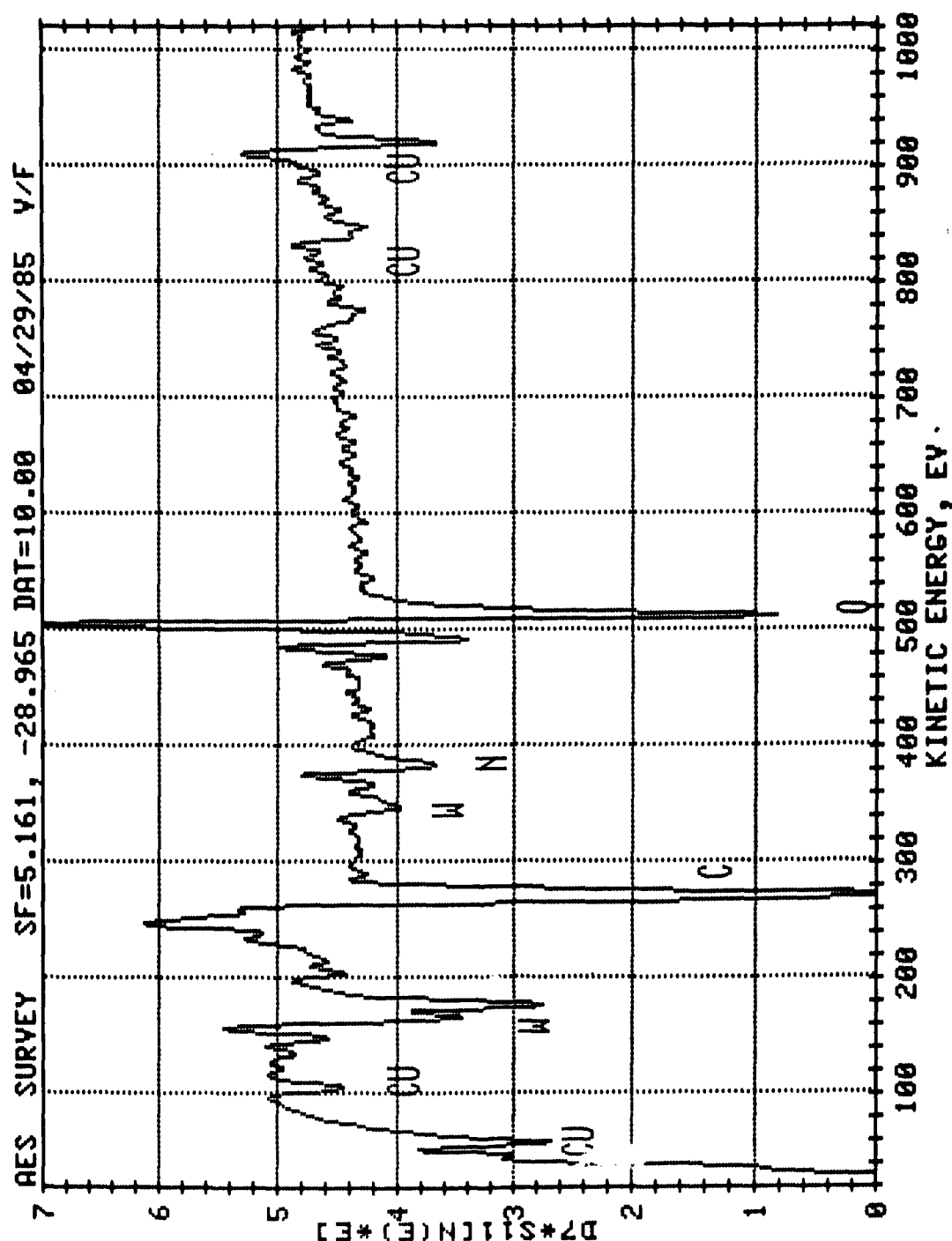FIGURE 5-19. AUGER ELECTRON SPECTRUM FROM UNIMPLANTED SURFACE OF 30W3 ELKONITE COUPON.
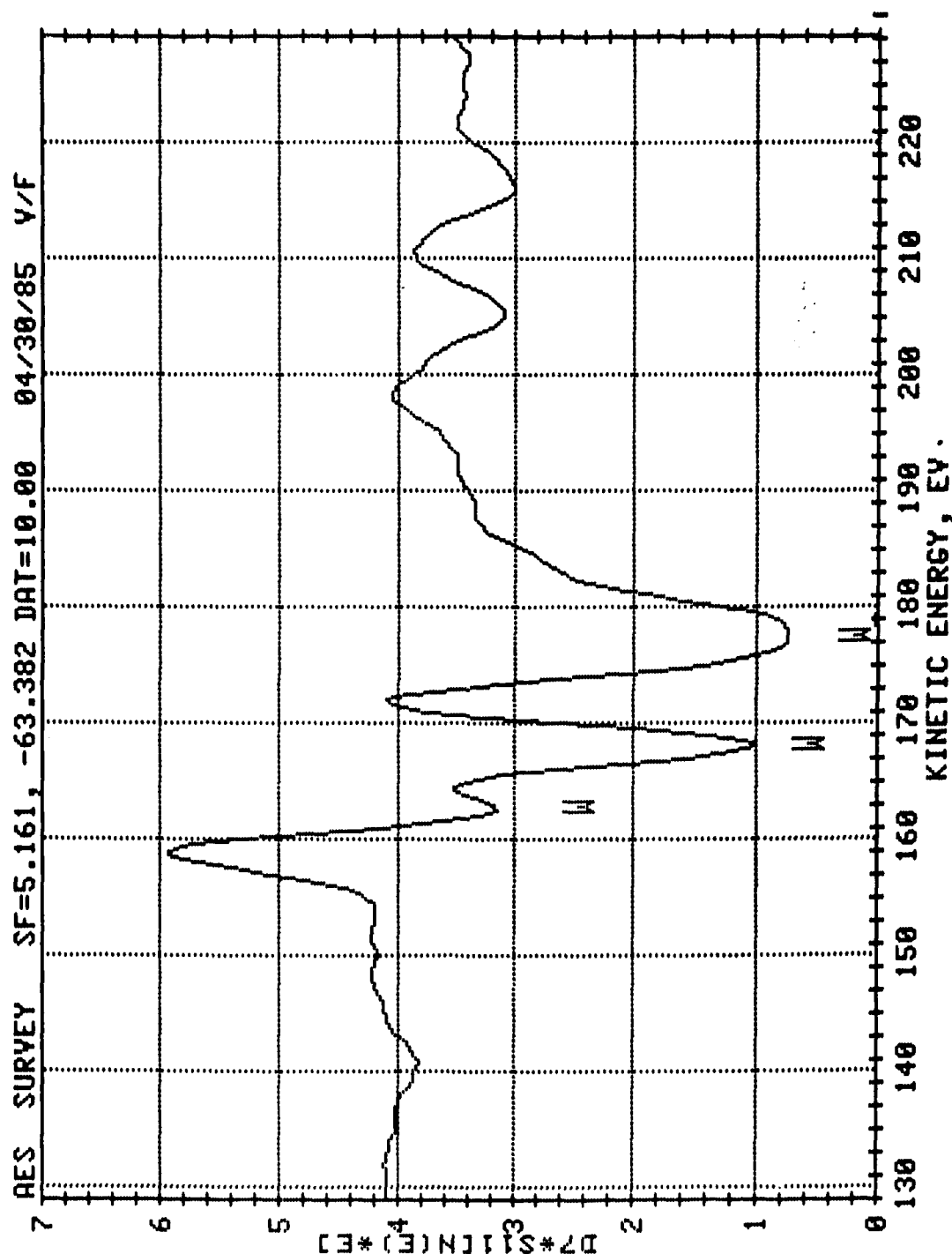
FIGURE 5-20. EXPANDED AES OF B-IMPLANTED COUPON AT A
SPUTTERING DEPTH OF APPROXIMATELY 75 nm. Boron
line at 179 eV is masked by tungsten spectrum.

SECTION 6
DISCUSSION

6.1 WEIGHT CHANGES AND SURFACE PROFILOMETRY

A companion of the measured weight changes shown in Table 5-1 and the estimated mass lost from the anode craters, Table 5-2, indicates that, in most cases, much of the mass lost from the crater was redeposited on the electrode. The major exception is the C-implanted anode, in which the mass estimate of the crater is 0.5 mg less than the measured weight change.

This quantitative difference between the C-implanted anode and the other electrodes, either B-implanted or unimplanted, can be explained if the material ejected from the crater of the C-implanted anode was preferentially copper and was not redeposited on the electrode's surface. Tungsten, with a much higher melting temperature and higher density than copper, would be expected to redeposit on the horizontal anode. Molten copper, on the other hand, may be more easily lost from the spark gap electrode region.

6.2 SEM, EDS AND AES ANALYSIS

The scanning electron microscopy, energy dispersive spectroscopy and Auger electron spectroscopy of the spark gap electrodes appear to support the conclusion that the C-implanted anode behaved differently from the others. First, SEM and EDS confirmed that the copper-colored spots on the anode and cathode electrodes were formed by molten droplets with a high percentage (up to 71 at. %) of copper. The droplets seen on the other electrodes appeared to have much higher concentrations of tungsten. Second, EDS analysis showed that melted areas inside the crater of the C-implanted anodes had very little Cu, as low as 11 at. %. A copper concentration of 19 at. % was measured for nodules in the crater of the B-implanted electrode, but the tungsten nodules may have been ejected and refallen into the crater, losing copper preferentially. This conclusion is supported by the SEM Robinson backscatter images inside the crater which indicate that the unimplanted and B-implanted anodes have considerably less high-Z material (W) than the crater of the C-implanted anode.

The Auger electron depth profiles of the crater region of the unimplanted and C-implanted anodes again indicate a strong difference in the relative concentrations of W and Cu. There is generally more W in the C-implanted anode over the approximately 10 nm sputtering depth than for the comparable profile in the unimplanted anode's crater.

6.3   IMPLANTATION PROFILE AND SURFACE SPUTTERING

The implantation of high doses of energetic C or B ions into the electrode material raises questions on the concentration and profile of the implanted species and on the amount of host material which is removed during the ion implantation process.

6.3.1   Computation of Implantation Profile

A simple computer code was used to calculate the average range and dispersion around the average, assuming that only classical Rutherford scattering is involved in stopping the ions. The density distribution of the implanted species is then a Gaussian, and no recoil injection or diffusion of the implanted material is included in the model.

In the computer model, the number density of the implanted species is distributed as,

$$n(x) = A \exp\left[\frac{-(x-R)^2}{2\sigma^2}\right] \qquad (2)$$

where

$$A = \frac{N}{\sigma}\sqrt{\frac{2}{\pi}}\left[1 - erf\left(\frac{R}{\sigma\sqrt{2}}\right)\right]^{-1} \qquad (3)$$

and R is the average range of implanted species, x the distance from the surface, N is the dose per unit area, and σ is the dispersion in range.

Table 6-1 shows the results of the calculations for 10^{18} cm^{-2} of 185 keV B and C implanted into pure W and Cu. It is clear that a Gaussian deposition profile is not realistic because the number density of solid W and Cu are 6.3×10^{22} cm^{-3} and 8.5×10^{22}, respectively. On the other hand, if all of the ions were distributed uniformly throughout a depth of the average range plus 2σ, then both the boron and carbon concentrations should be on the order of one-third to half that of the tungsten or copper. It thus appears that a large percentage of the tungsten surface should have been converted to tungsten carbides or borides.

-39-

TABLE 6-1. CALCULATED IMPLANTATION PARAMETERS FOR
NORMALLY INCIDENT 185 kV IONS

Implant/ Host	Range (nm)	Sigma* (nm)	n(0)* (cm^{-3})	n(R)* (cm^{-3})	n** (cm^{-3})
C$^+$/W	147	101	1.9×10^{23}	5.4×10^{23}	2.9×10^{22}
B$^+$/W	181	119	1.6×10^{23}	5.2×1^{23}	2.4×10^{22}
C$^+$/Cu	215	75.5	4.2×10^{23}	2.4×10^{25}	2.7×10^{22}
B$^+$/Cu	259	86.7	3.8×10^{23}	3.3×10^{25}	2.3×10^{22}

* Assuming Gaussian deposition profile.

** Average density assuming 10^{18} ions/cm^2 implanted uniformly over a depth of R + 2 .

6.3.2 Surface Sputtering

Sputtering yields for C$^+$ or B$^+$ on W or Cu are not available in the literature. However, empirical extrapolations[15] of lower energy data for N$^+$ and O$^+$ on W and Cu targets indicate that they should be in the range of 0.1 to 0.2 W atom/ion and 0.3 to 0.5 Cu atom/ion at 185 keV. Thus a 10^{18} cm^{-2} incident dose of 185 keV B$^+$ or C$^+$ ions may sputter as much as 30 nm of W or 60 nm of Cu. These are small fractions of the range of the implanted ions, so that sputtering during ion implantation can be neglected to first approximation.

SECTION 7
CONCLUSIONS

Ion implantation of carbon into W-Cu spark gap electrodes has reduced the mass loss per coulomb by approximately a factor of 2, and based on the volume of the central crater in the anode electrode, by about a factor of 4. This is a very encouraging result of the Phase I program.

Although the mass lost per coulomb from boron-implanted electrodes was comparable to the C-implants, the crater volume was almost identical to the unimplanted control sample. The discrepancies between crater volume and mass loss are likely due to redeposition of crater material onto the sides of the anode electrode.

The effect of the implanted carbon in reducing spark gap electrode erosion apparently is a result of the higher enthalpy to melt WC than for pure W. This difference in the physical properties of the surface of the C-implanted electrodes would allow more heat to be dissipated by the arc at the surface before the onset of melting. Furthermore, the thermal diffusivity of WC at its melting temperature is approximately a factor of six greater than for pure W. Heat input to WC is thus transferred more quickly to the bulk material than for the unimplanted electrodes.

We do not have enough information on the thermal properties of tungsten borides to understand the apparent failure of boron implantation to reduce spark gap electrode erosion. It is also possible that chemical reactions between the implanted boron and the highly excited nitrogen and oxygen plasma in the arc may remove the boron from the tungsten during the discharge.

REFERENCES

1. T.R. Burkes, M.O. Hagler, M. Kristiansen, J.P. Craig, W.M. Portnoy, and E.E. Kunhart, "A Critical Analysis and Assessment of High Power Switches", Vol. 1, Report No. NP30/78, Naval Surface Weapons Center, Dahlgren, VA (Sept., 1978), pp. 233-265.

2. J.E. Gruber and R. Suess, "Investigation of the Erosion Phenomenon in High Current, High Pressure Gas Discharges", IPP 4/72, Institut fur Plasmaphysyk, Garsching, Germany, (Dec., 1969).

3. D. Johnson and E. Pfender, "Modeling and Measurement of the Initial Anode Heat Fluxes in Pulsed High Current Arcs", IEEE Trans, Plasma Sci., PS-7, 44, (1979).

4. R.A. Petr and T.R. Burkes, "Erosion of Spark Gap Electrodes", IEEE Trans. Plasma Sci., PS-8, 149, (1980).

5. L.B. Gordon, M. Kristiansen, M.O. Hagler, H.C. Kirbie, R.M. Ness, L.L. Hatfield and J.N. Marx, "Material Studies in a High Energy Spark Gap", IEEE Trans. Plasma Sci., PS-10, 286, (1982).

6. A.L. Donaldson, M.O. Hagler, M. Kristiansen, G. Jackson and L. Hatfield, "Electrode Erosion Phenomena in a High Energy Pulsed Discharge", IEEE Trans. Plasma Sci., PS-12, 28, (1984).

7. M. Kristiansen, Texas Tech. University, private communication, (May, 1985).

8. W.H. Childs, "Thermophysical Properties of Selected Space-Related Materials", The Aerospace Corp., El Segundo, CA, Report No. TOR-0081(6435-02)-1, (Feb., 1981).

9. R.C. Weast, ed., CRC Handbook of Chemistry and Physics, 59th Edition, CRC Press, W. Palm Beach, FL, pp.D-51, (1977).

10. J.K. Hirvonen, "Ion Implantation in Tribology and Corrosion Science", J. Vac. Sci. Technol., 15, 1662, (1978).

11. Trademark of CMW, Inc., Indianapolis, IN.

12. J.J. Moriarty, H.I. Milde and J.E. Hipple, "Multimegavolt Modulator Study", Rome Air Development Center, Hanscom AFB, MA, Report No. RADC-TR-70-107, (1970).

13. R.G. Masters, PhotoMetrics, Inc., private communication, (May, 1985).

14. P.W. Palmberg, et at., "Handbook of Auger Electron Spectroscopy", Physical Electronics Industries, Inc., Edina, MN, (Feb., 1972).

15. N. Matsunami, et al., "Energy Dependence of the Ion-Induced Sputtering Yields of Monatomic Solids", At. Data and Nuc. Data Tables, 31, 1, (1984).

END

FILMED

11-85

DTIC